International Journal of Heat and Mass Transfer 62 (2013) 314–322

Contents lists available at SciVerse ScienceDirect

International Journal of Heat and Mass Transfer

journal homepage: www.elsevier.com/locate/ijhmt

Closed form solutions of the heat diffusion equation with a Gaussian source

T. Antonakakis [a,b,*], C. Maglioni [a], V. Vlachoudis [a]

[a] European Organization for Nuclear Research, CERN CH-1211, Genève 23, Switzerland
[b] Department of Mathematics, Imperial College, London SW7 2AZ, UK

ARTICLE INFO

Article history:
Received 14 September 2012
Received in revised form 24 February 2013
Accepted 26 February 2013
Available online 9 April 2013

Keywords:
Analytical solution
Infinite medium
Gaussian heat source
Transient temperature

ABSTRACT

In the context of the Large Hadron Collider, high energy particles are dumped onto blocks of material that are commonly called beam-dumps. The high energy deposition is almost instantaneous and can be represented by a very high power source for a short period of time. Temperatures can rise above failure limits at the locations of highest energy deposition. Particle beam accelerators are also widely used for medical applications where electron, proton or ion particle beams at energies of the order of megaelectronvolts are used to destroy cancer cells [1]. The motivation of this article is to be able to calculate the temperature fields without turning to numerical simulations that can be very time consuming. We present closed form solutions of the transient heat diffusion problem during the energy deposition. The transient heat diffusion equation assumes infinitely fast propagation of the information throughout the medium, but the diffusion process remains at finite speeds. Energy is deposited in such a small time interval so that the heat flux across the boundaries is assumed to be zero. It follows that the heat diffusion equation can be solved in an infinite medium, by the use of Green's functions, to provide closed form solutions for the transient temperature field within the pulse time. The range of applicability of these solutions is supported by a parametric relative error analysis. They demand very little computational power and time compared to commercial numerical software.

1. Introduction

An important issue in beam accelerator technology is the actual dumping of the beam where eventually the particle beam needs to be absorbed into a material of specific density. Energy is then deposited in form of heat within a time interval of the order of microseconds or even nanoseconds. The power source's spatial distribution has many variants, but can be modelled as Gaussian and the temporal dependence can be assumed constant. The pulse-length denotes the time interval in which energy is deposited in the material block from the accelerated particle beam. The width of the Gaussian plays a key role in the maximum energy deposited per unit volume and by consequence to the maximum temperature and temperature gradient. In the timescale of the beam's pulse-length, the size and location of the intercepted beam allow us to assume thermal diffusion in infinite media. At CERN there are hundreds of material blocks dedicated to absorb particle beams with energies ranging from a few keV to 7 TeV. At these energies, with dense enough materials and small enough beam distributions, temperatures can rise to the point of phase change [28]. For lower densities where phase change does not happen, temperatures can still rise enough to reach structural failure [24]. Melting point criteria and static stresses are a direct consequence of the resulting temperature field that can result in failure. On the other hand quasi-static stresses, and dynamic stresses induced by the almost instantaneous temperature field and temperature gradient field pose a much bigger problem [24,27,28]. For a precise evaluation of the stresses within the solid one needs the exact temperature field and its variation in time. Heat conduction in infinite bodies with concentrated sources is a well known subject [6,8]. Point and line sources [25] and uniformly distributed circular sources respectively overestimate and underestimate the temperature field and gradients resulting from a Gaussian distributed source. [18] presents closed form solutions for the maximum temperature rise caused by a Gaussian laser beam. Furthermore Gaussian distributed moving sources have been studied in [26], but no closed form solutions have been given for finite [4,11,17,31] or semi-infinite bodies [12,13,22]. Finally [19] presents analytical solutions to quasi-steady-state temperature distributions where the moving circular Gaussian heat source is taken into account through the boundary conditions. The goal of this article is to provide closed form solutions in infinite spaces, of the parabolic heat conduction equation with power sources of Gaussian distribution in space and constant in time together with a parametric error analysis necessary for the usability of such solutions. In order to obtain closed

* Corresponding author at: European Organization for Nuclear Research, CERN CH-1211, Genève 23, Switzerland.
E-mail addresses: tryfon.antonakakis@cern.ch, tryfon.antonakakis09@imperial.ac.uk (T. Antonakakis).

0017-9310/$ - see front matter © 2013 Elsevier Ltd. All rights reserved.
http://dx.doi.org/10.1016/j.ijheatmasstransfer.2013.02.061

Nomenclature

θ	temperature
ρ	density
k	thermal conductivity
c	specific heat
A	peak of power density function
t_p	pulselength
σ	standard deviation of Gaussian power density
Π_1	non-dimensional thermal diffusivity
Π_2	non-dimensional standard deviation of Gaussian power density
Π_3	peak of non-dimensional power density function
E_L	relative energy loss
ϵ_{nrms}	normalized root mean square error for the series solutions
E_{nrms}	normalized root mean square error between infinite space solutions and partial sums solutions
E_{max}	normalized maximum error between infinite space solutions and partial sums solutions

form solutions we assume an equivalent standard deviation in all directions, σ, equal to the geometric average of the real standard deviations. The relations obtained are in terms of well known functions which can easily be computed using any mathematical software. Furthermore we obtain relations of elementary functions for the peak temperatures which are very important for the design of beam intercepting devices or any other bodies dedicated to intercept a beam.

It is important to relate the analytical solutions with the possible practical applications. At first we will solve for three, two and one dimensional geometries for infinite spaces then compare their non-dimensional form with the analytical formulations obtained from infinite series solutions for finite domains with Neumann type boundary conditions. The number of terms in the partial sum of the series will indicate the precision of the approximation and can turn to be expensive in terms of computing time. Finally we will quantify the limits of our assumption – size of the Gaussian power source, pulselength, energy, thermal conductivity, etc. – to benchmark the suitability of this model for real bounded geometries. Throughout the article solutions will be presented in a decreasing dimensional order.

2. Problem description

When a particle beam intercepts a target material the energy is deposited in one of many ways depending on the geometry of the target, the density of the material, the size and energy of the beam. For a short enough pulselength, the heat flux across surfaces far away from the source is close to zero since temperature gradients at those locations are nearly null. By consequence the solution of the transient heat diffusion equation in infinite media for time intervals of the order of the pulselength provides a very good approximation to the real bounded problem with Neumann boundary conditions.

The first case treated consists in the energy deposition having a spherical Gaussian distribution, located within the solid and distant enough from the boundaries. This type of geometry and beam is illustrated in Fig. 1(a) and will be noted as case **A**. The beam's power deposition is modelled to be very small throughout the medium until it peaks almost instantaneously in a spherically Gaussian manner.

Next we consider a two dimensional infinite space, say the plane (Oxy) of Fig. 1(b) and (c) where the source is modelled by a two dimensional Gaussian distribution. Let us note this case as case **B**. A real three dimensional problem can be modelled as one of case **B** if the gradients of the source term with respect to z are nearly zero. This would be the case of a long cylinder along the z axis, with radius $r \gg \sigma$ and a Gaussian energy deposition in the (Oxy) plane. Case **B** can also be applied for a very thin object where the thickness is in the z direction and the gradients in that direction are close to zero. Note that for the very thin object the boundary conditions at the faces parallel to the (Oxy) plane would not affect the solution from a convection point of view for short times of the order of the beam's pulselength. On the other hand one should be more careful in the case of very high temperatures where, heat transfer by radiation takes place. Case **B** is illustrated in Fig. 1(c).

Finally we consider in case **C** a one dimensional infinite space, the line (Ox), where the source is modelled by a one dimensional Gaussian distribution. Fig. 1(d) illustrates case **C**. The particle beam in the (Oz) direction traverses a thin sheet of material in the (Oxz) plane. If the gradients of the power source along z are nearly zero then the only non-trivial gradients of temperature will be along x. Another application of the one dimensional model is when a beam in (Oz) traverses a wire in (Ox) and the beam's width is larger then the wire's diameter.

3. Analytical solutions for infinite media

The classical equation of heat diffusion is,

$$\frac{\partial\theta(\mathbf{r},t)}{\partial t} - D\nabla^2\theta(\mathbf{r},t) = f(\mathbf{r},t) \quad \text{for} \quad 0 < t < t_p \quad \text{and} \quad \mathbf{r} = (x,y,z), \tag{1}$$

where $D = k/\rho c_v$ and $f(\mathbf{r},t) = g(\mathbf{r},t)/\rho c$. ρ, k,c and $g(\mathbf{r},t)$ respectively represent the density, thermal conductivity, specific heat and the power source. The power source is in $\mathrm{W}\cdot\mathrm{m}^{-3}$ that represent a power density. All parameters are in *SI* units. The pulselength, t_p, represents the end of the energy deposition and is usually of the order of μs. Finally $\theta(\mathbf{r},t) = T(\mathbf{r},t) - T_i$ where T_i is the initial temperature and $T(\mathbf{r},t)$ is the temperature field in space and time. The initial condition for Eq. (1) is $\theta(\mathbf{r},0) = 0$ Let us now solve this equation considering three different power sources, hence three different variants of the function $g(\mathbf{r})$. The Green's function for the diffusion problem in an infinite medium in n dimensions is [6],

$$G_n(\mathbf{R},\tau) = H(\tau)\frac{1}{(4\pi D\tau)^{n/2}}e^{\frac{-\mathbf{R}^2}{4D\tau}}, \tag{2}$$

where $\mathbf{R} = \mathbf{r} - \mathbf{r}'$ and $\tau = t - t'$ and H represents the Heaviside function. The general approach using Green's functions yields the following general solutions [6]

$$\theta(\mathbf{r},t) = \int_{t_0}^{t}\int_V G_n(\mathbf{R},\tau)f(\mathbf{r}',t')dV'dt' + \int_V G_n(\mathbf{R},t-t_0)\theta(\mathbf{r}',t_0)dV'. \tag{3}$$

The initial conditions are assumed homogeneous so that the second integral of Eq. (3) is zero. The space integral of the first term is the convolution of two Gaussian functions with zero mean and is therefore a Gaussian itself with zero mean and a standard deviation equal to $\sigma_{G\circledast f} = \sqrt{(\sigma^2 + 2D\tau)}$ [30]. Following the time integration one obtains solutions for the transient heat diffusion problem with

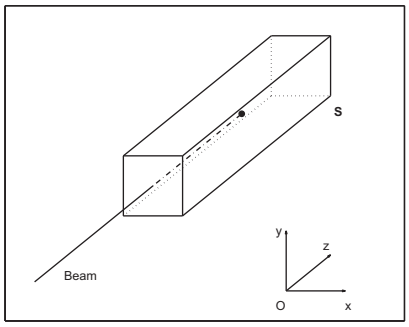

(a) The particle beam enters the solid **S** and is stopped at the thick dot, where most of its energy is deposited in forms of a heat source with a Gaussian distribution.

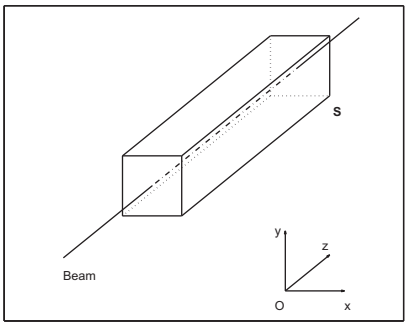

(b) The particle beam enters the solid **S** and goes right through. Energy is uniformly distributed in the (Oz) direction but follows a Gaussian distribution in the (Oxy) plane.

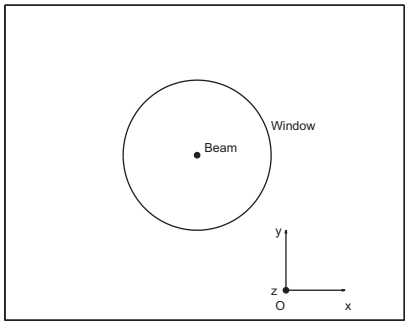

(c) The particle beam parallel to the (Oz) axis traverses the thin window oriented in plane (Oxy). The energy deposition distribution is Gaussian and in plane (Oxy).

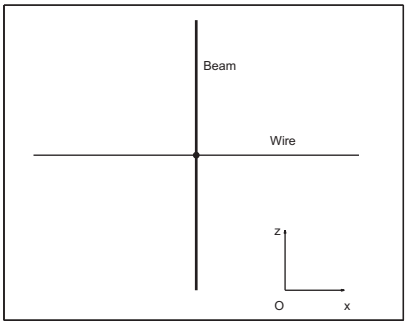

(d) The particle beam parallel to the (Oz) axis traverses the wire oriented in the (Ox) direction. Energy deposition has a Gaussian distribution in the (Ox) direction.

Fig. 1. Illustration of beam and beam intercepting devices that can be modelled as three, two or one dimensional. (a) The particle beam enters the solid **S** and is stopped at the thick dot, where most of its energy is deposited in forms of a heat source with a Gaussian distribution. (b) The particle beam enters the solid **S** and goes right through. Energy is uniformly distributed in the (*Oz*) direction but follows a Gaussian distribution in the (*Oxy*) plane. (c) The particle beam parallel to the (*Oz*) axis traverses the thin window oriented in plane (*Oxy*). The energy deposition distri-bution is Gaussian and in plane (*Oxy*). (d) The particle beam parallel to the (*Oz*) axis traverses the wire oriented in the (*Ox*) direction. Energy deposition has a Gaussian distribution in the (*Ox*) direction.

respect to well known functions namely the exponential, the error function and the exponential integral. Moreover these solutions simplify to operations of elementary functions for the computation of temperature peaks that happen at the location of $\mathbf{r} = 0$. The development of the first integral term of Eq. (3) is shown in the appendix.

3.1. Case A

This case is applied for specific energy beams and material densities where the power deposition peaks at a specific location, far enough from the boundaries in a spherical Gaussian distribution. The source term in Eq. (1) is then of the form, $g(\mathbf{r},t) = A\exp\left(\frac{-r^2}{2\sigma^2}\right)$. Where A quantifies the total power density and σ represents the standard deviation of the Gaussian. The solution to Eq. (1) by performing the necessary integrations reads,

$$\theta_A(r,t) = A\frac{\sqrt{2\pi}}{2}\frac{\sigma^3}{k}\frac{1}{r}\left(\operatorname{erf}\left(\frac{r}{\sqrt{2\sigma^2}}\right) - \operatorname{erf}\left(\frac{r}{\sqrt{2\sigma^2+4Dt}}\right)\right), \tag{4}$$

where r represents the radial coordinate since the source term is independent of both spherical angles and the error function is defined as $\operatorname{erf}(x) = \int_o^x e^{-t^2}dt$. One can notice that the above solution is not defined for $r = 0$, however the peak of temperature is expected at that location. To obtain a closed form for the temperature at $r = 0$, we expand Eq. (4) by the use of MacLaurin series and then take the limit as $r \to 0$. We then obtain,

$$\theta_A(0,t) = A\sqrt{2}\frac{\sigma^3}{k}\left(\frac{1}{\sqrt{2\sigma^2}} - \frac{1}{\sqrt{2\sigma^2+4Dt}}\right). \tag{5}$$

3.2. Case B

This case is applied when the power deposition does not vary with respect to z. The source term in Eq. (1) is of the form, $g(\mathbf{r},t) = A\exp(\frac{-(x^2+y^2)}{2\sigma^2})$. Where A quantifies the total power density in $W\cdot m^{-3}$ and σ represents the standard deviation of the Gaussian. The solution to Eq. (1) by performing the necessary integrations reads,

$$\theta_B(r,t) = -\frac{A}{2}\frac{\sigma^2}{k}\left(\operatorname{Ei}\left(1,\frac{r^2}{2\sigma^2}\right) - \operatorname{Ei}\left(1,\frac{r^2}{2\sigma^2+4Dt}\right)\right), \tag{6}$$

where $r^2 = x^2 + y^2$ and $\operatorname{Ei}(1,z) = \int_1^\infty \frac{e^{-tz}}{t}dt$, the exponential integral. In order to obtain the value of the temperature field in time for $r = 0$ we need to take the limit of the right hand side of Eq. (6) for $r \to 0$. It is obtained by expanding in McLaurin series the exponential integral function and then taking the limit as $r \to 0$. We obtain,

$$\theta_B(0,t) = -\frac{A}{2}\frac{\sigma^2}{k}\ln\left(\frac{2\sigma^2}{2\sigma^2+4Dt}\right). \tag{7}$$

3.3. Case C

The source term in Eq. (1) is of the form, $g(z,t) = A\exp\left(\frac{-z^2}{2\sigma^2}\right)$. Where A quantifies the total power density and σ represents the standard deviation of the Gaussian. The solution to Eq. (1) by performing the necessary integrations reads,

$$\theta_C(z,t) = -\frac{\sqrt{2}}{2}\frac{A\sigma}{k}\left(z\sqrt{\pi}\left(\operatorname{erf}\left(\frac{z}{\sqrt{2\sigma^2}}\right) - \operatorname{erf}\left(\frac{z}{\sqrt{2\sigma^2+4Dt}}\right)\right) + \sqrt{2\sigma^2}\exp\left(\frac{-z^2}{2\sigma^2}\right) - \sqrt{2\sigma^2+4Dt}\exp\left(\frac{-z^2}{2\sigma^2+4Dt}\right)\right). \quad (8)$$

The maximum temperature occurring at $z = 0$ is easily obtained by,

$$\theta_C(0,t) = -\frac{\sqrt{2}}{2}\frac{A\sigma}{k}\left(\sqrt{2\sigma^2} - \sqrt{2\sigma^2+4Dt}\right). \quad (9)$$

4. Limits of the infinite medium assumption

The formulations in the above paragraph are only useful if one knows their limits of applicability. One needs to know to what extent the above formulations will yield correct results in comparison to finite domains with Neumann type boundary conditions. In order to analyze the limits of the above solutions we will non-dimensionalize the problem in the following way. We will choose the reference length to be L where its value will depend on the real bounded problem's characteristic length. The reference time is set as t_p and the reference temperature is set as T_i, the body's initial temperature. We then obtain the following dimensionless variables that read,

$$\mathbf{r}^* = \frac{\mathbf{r}}{L}, \quad t^* = \frac{t}{t_p} \quad \text{and} \quad \theta^* = \frac{\theta}{T_i}. \quad (10)$$

Inserting the above variables into Eq. (1) and dropping the star notation from now on, we obtain the following dimensionless equation,

$$\frac{\partial\theta}{\partial t} - \Pi_1\nabla^2\theta = \Pi_3\exp\left(-\frac{\mathbf{r}\cdot\mathbf{r}}{2\Pi_2^2}\right), \quad (11)$$

where Π_1, Π_2 and Π_3 are three dimensionless parameters yielding,

$$\Pi_1 = \frac{Dt_p}{L^2}, \quad (12)$$

$$\Pi_2 = \frac{\sigma}{L}, \quad (13)$$

$$\Pi_3 = \frac{At_p}{\rho c_p T_i}. \quad (14)$$

All the parameters used to describe thermal properties of the intercepting body, beam characteristics and geometry of the intercepting body are incorporated without loss of generality into Eqs. (12)–(14). Note that these parameters can also be obtained using the Π-Buckingham theorem. The exact solutions for the infinite medium in their dimensionless form read,

$$\theta_A(r,t) = \frac{\sqrt{2\pi}}{2}\frac{\Pi_2^3\Pi_3}{\Pi_1}\frac{1}{r}\left(\operatorname{erf}\left(\frac{r}{\sqrt{2\Pi_2^2}}\right) - \operatorname{erf}\left(\frac{r}{\sqrt{2\Pi_2^2+4\Pi_1 t}}\right)\right), \quad (15)$$

$$\theta_B(r,t) = -\frac{1}{2}\frac{\Pi_2^2\Pi_3}{\Pi_1}\left(\operatorname{Ei}\left(1,\frac{r^2}{2\Pi_2^2}\right) - \operatorname{Ei}\left(1,\frac{r^2}{2\Pi_2^2+4\Pi_1 t}\right)\right), \quad (16)$$

$$\theta_C(z,t) = -\frac{\Pi_2\Pi_3}{\Pi_1}\left(\frac{\sqrt{2\pi}}{2}z\left(\operatorname{erf}\left(\frac{z}{\sqrt{2\Pi_2^2}}\right) - \operatorname{erf}\left(\frac{z}{\sqrt{2\Pi_2^2+4\Pi_1 t}}\right)\right) + \Pi_2\exp\left(\frac{-z^2}{2\Pi_2^2}\right) - \frac{\sqrt{2}}{2}\sqrt{2\Pi_2^2+4\Pi_1 t}\exp\left(\frac{-z^2}{2\Pi_2^2+4\Pi_1 t}\right)\right). \quad (17)$$

The respective maximum temperatures in non-dimensional form are,

$$\theta_A(0,t) = \Pi_3\sqrt{2}\frac{\Pi_2^3}{\Pi_1}\left(\frac{1}{\sqrt{2\Pi_2^2}} - \frac{1}{\sqrt{2\Pi_2^2+4\Pi_1 t}}\right). \quad (18)$$

$$\theta_B(0,t) = -\frac{\Pi_3}{2}\frac{\Pi_2^2}{\Pi_1}\ln\left(\frac{2\Pi_2^2}{2\Pi_2^2+4\Pi_1 t}\right). \quad (19)$$

$$\theta_C(0,t) = -\frac{\sqrt{2}}{2}\frac{\Pi_3\Pi_2}{\Pi_1}\left(\sqrt{2\Pi_2^2} - \sqrt{2\Pi_2^2+4\Pi_1 t}\right). \quad (20)$$

The ratio of Eqs. (18)–(20) to Π_3 is shown in panels (b), (d) and (f) of Fig. 2 for varying Π_1 and Π_2. They are used to determine whether the adiabatic temperature peak Π_3 is a good approximation for the real temperature peak.

We will use the relative energy difference between the total energy injected in the infinite system and the energy inside the confined normalized space, in order to restrict the intervals of applicability of the infinite space solutions in a normalized finite space. The relative energy loss reads,

$$E_L(t) = \frac{\int_V \theta(\mathbf{r},t)dV - \int_{V_\infty} tf(\mathbf{r},t)dV}{\int_{V_\infty} tf(\mathbf{r},t)dV}, \quad (21)$$

where $\theta(\mathbf{r},t)$ is the solution of Eqs. (15)–(17). The denominator of Eq. (21) represents the total energy inserted in the infinite space within the time interval $[0,t]$ where $t \in [0,1]$. It is obvious that Π_3 simplifies and we are only left with Π_1 and Π_2 as varying parameters in $E_L(t)$. Log–log scale contour plots of E_L versus Π_1 and Π_2 are presented in Fig. 2(a), (c) and (e) respectively for the three, two and one dimensional solutions. The intervals of the varying parameters Π_1 and Π_2 are chosen to illustrate most engineering situations but also show the limitations of the infinite medium assumption. Indeed by computing the parameters Π_1 and Π_2 one can directly know the expected relative energy error and decide whether the infinite medium formulation is valid or not. Instinctively, smaller values of Π_1, that translate into the diffusion time being much smaller then the pulselength, yield almost no heat loss through the boundaries and the same goes for smaller values of Π_2 where the energy deposition width gets smaller with respect to the characteristic length of the object. If E_L is within the darkest regions of Fig. 2(a), (c) or (e) then the limit of applicability of the infinite space solutions for a finite domain is reached. On the other hand if the relative energy loss is below a specific value one can use the infinite medium assumption within a known accuracy in terms of energy loss. If one chooses to evaluate the total energy loss through the boundaries of the normalized finite domain, then computing the numerator of Eq. (21) would suffice and Π_3 parameter would be taken into account.

5. Series solutions

Infinite series solutions to transient heat diffusion problems in simple geometries are generally known and will here be used for comparison purposes only. Solution of the heat diffusion equation for a finite domain can be found using Sturm–Liouville theory [16]. We briefly present the infinite series solutions for Eq. (11). For one dimension the definition interval is, $z \in [-1,1]$, for two and three dimensions the space domain is, $r \in [0,1]$. The conditions at the boundaries are of type Neumann and the initial conditions are homogeneous. The solution of Eq. (11) is of the form $u = \sum_{n=0}^{\infty} A_n(t)\Phi_n$, where $A_n(t) = \frac{K_n}{\beta_n^2}\left(1 - \exp\left(-\beta_n^2 t\right)\right)$ for $n = 1,2,\ldots$, and Φ_n are the eigenfunctions for the respective homogeneous problem. $\beta_n^2 = \Pi_1\lambda_n^2$ where λ_n represents the eigenvalues of the homogeneous heat diffusion problem and will be defined for each dimensional case. Since the boundary conditions are of Neumann type we also have a zero eigensolution that yields $A_0(t) = K_0 t$. K_n

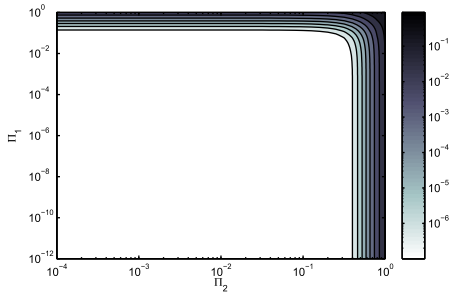

(a) Relative energy loss out of a normalized unit sphere applicable to case **A** of section 2.

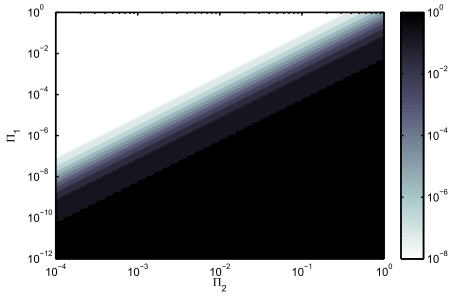

(b) Ratio of non-dimensional peak temperature to the theoretical value assuming zero diffusivity

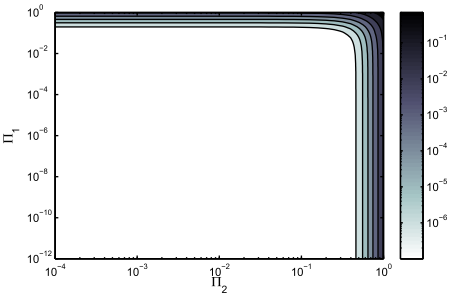

(c) Relative energy loss out of a normalized unit disc applicable to case **B** of section 2.

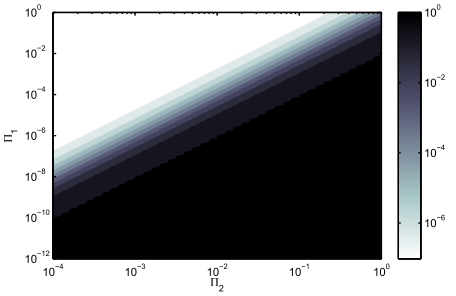

(d) Ratio of non-dimensional peak temperature to the theoretical value assuming zero diffusivity

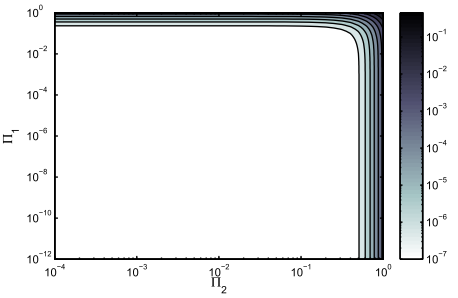

(e) Relative energy loss out of a normalized segment of length 2 applicable to case **C** of section 2.

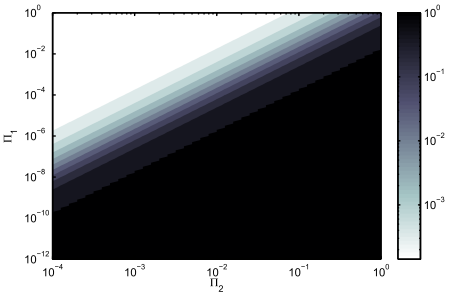

(f) Ratio of non-dimensional peak temperature to the theoretical value assuming zero diffusivity.

Fig. 2. The present figure is organized in a way that the three rows in descending order respectively represent cases **A**, **B** and **C**. It shows relative heat flow contours E_L of Eq. (21) versus parameters Π_1 and Π_2 in panels (a), (c) and (e). Each of these panels represents the heat flow across an imaginary surface of radius one for panels (a) and (c) and length two for panel (e) representing the one dimensional case. Panels (b), (d) and (f) show the sensibility of the peak temperature compared to the theoretical peak for a zero diffusivity by plotting the ratio of Eqs. (18)–(20) for $t = 1$ to Π_3. (a) Relative energy loss out of a normalized unit sphere applicable to case **A** of Section 2. (b) Ratio of non-dimensional peak temperature to the theoretical value assuming zero diffusivity. (c) Relative energy loss out of a normalized unit disc applicable to case **B** of Section 2. (d) Ratio of non-dimensional peak temperature to the theoretical value assuming zero diffusivity. (e) Relative energy loss out of a normalized segment of length 2 applicable to case **C** of Section 2. (f) Ratio of non-dimensional peak temperature to the theoretical value assuming zero diffusivity.

coefficients are presented in the following paragraphs. Let us now treat each case separately.

5.1. 3D spherical Bessel series expansion

The temperature field varying in space and time yields the infinite series solution,

$$u(r,t) = A_0(t) + \sum_{n=1}^{\infty} A_n(t) j_0(\lambda_n r), \tag{22}$$

where λ_n is the solution of the following equation, $\lambda_n j_1(\lambda_n) = 0$ and K_n has the following form,

$$\begin{aligned} K_0 &= 3\int_0^1 \Pi_3 \exp\left(\frac{-r^2}{2\Pi_2^2}\right) r^2 dr, \\ K_n &= \frac{2\Pi_3 \int_0^1 j_0(\lambda_n r) \exp\left(\frac{-r^2}{2\Pi_2^2}\right) r^2 dr}{\int_0^1 (j_0(\lambda_n r))^2 r^2 dr}. \end{aligned} \tag{23}$$

5.2. 2D Bessel series expansion

The temperature field varying in space and time yields the infinite series solution,

$$u(r,t) = A_0(t) + \sum_{n=1}^{\infty} A_n(t) J_0(\lambda_n r), \tag{24}$$

where λ_n is the solution of the following equation, $J_1(\lambda_n) = 0$ and K_n has the following form,

$$\begin{aligned} K_0 &= 2\int_0^1 \Pi_3 \exp\left(\frac{-r^2}{2\Pi_2^2}\right) r dr, \\ K_n &= \frac{2\Pi_3 \int_0^1 J_0(\lambda_n r) \exp\left(\frac{-r^2}{2\Pi_2^2}\right) r dr}{(J_0(\lambda_n))^2}. \end{aligned} \tag{25}$$

5.3. 1D Fourier series expansion

The temperature field varying in space and time yields the infinite series solution,

$$u(z,t) = A_0(t) + \sum_{n=1}^{\infty} A_n(t) \cos(n\pi z), \tag{26}$$

where $\lambda_n = n\pi$ and

$$\begin{aligned} K_0 &= \frac{1}{2}\Pi_3 \int_{-1}^{1} \exp\left(\frac{-z^2}{2\Pi_2^2}\right) dz, \\ K_n &= \Pi_3 \int_{-1}^{1} \cos(n\pi z) \exp\left(\frac{-z^2}{2\Pi_2^2}\right) dz. \end{aligned} \tag{27}$$

5.4. Accuracy of the partial sum solutions

The partial sum series solutions will be used to compare with the infinite medium solutions. The three independent parameters in the diffusion equation play a major role into choosing the number of terms necessary to achieve a satisfying accuracy for the partial sum. One way to achieve this is by taking into account Bessel's Inequality [29] which yields a value for the root mean square error of the temperature field. Provided that the function u behaves well enough which is the case for the present problem, we can write,

$$\sum_{n=0}^{\infty} A_n(t)^2 \int_V \Phi_n(\mathbf{r})^2 dV = \int_V (t \cdot f(\mathbf{r},t))^2 dV. \tag{28}$$

If instead of the infinite sum we take a partial sum then the equality becomes Bessel's inequality. It is then possible to evaluate the accuracy of our solution depending on the number of terms in the partial sum by using the normalized root mean square error ϵ_{nrms} as,

$$\begin{aligned} \epsilon_{nrms}(t) = &\frac{1}{max(tf(\mathbf{r},t),\mathbf{r})} \\ &\times \frac{1}{\sqrt{V}} \left(\int_V (t \cdot f(\mathbf{r},t))^2 dV - \sum_{n=0}^{m} A_n(t)^2 \int_V \Phi_n(\mathbf{r})^2 dV \right)^{\frac{1}{2}}. \end{aligned} \tag{29}$$

5.5. Comparison of the closed form solutions with the partial sum solutions

Paragraph Section 4 will ensure to the desired accuracy the validity of the Neumann boundary condition but one wishes to verify that the temperature field of the infinite solutions within the normalized space matches well enough the according field for the partial sum solutions. To this end we will define a normalized root mean square error between the infinite space solutions and the finite space partial sums as E_{nrms} and a normalized maximum error E_{max}. Let θ and u_n represent respectively the infinite space and the partial sum solutions such that the errors respectively read,

$$E_{nrms}(t) = \frac{1}{max(u_n(\mathbf{r},t),\mathbf{r})} \left(\frac{1}{V} \int_V (\theta(\mathbf{r},t) - u_n(\mathbf{r},t))^2 dV \right)^{\frac{1}{2}}, \tag{30}$$

$$E_{max}(t) = \frac{max(|\theta(\mathbf{r},t) - u_n(\mathbf{r},t)|,\mathbf{r})}{max(u_n(\mathbf{r},t),\mathbf{r})}. \tag{31}$$

The errors will be computed for several values of t within the normalized time interval $[0,1]$. Note that the actual volume integral becomes a one-dimensional integral for all three dimensional cases.

6. Case studies and validation of the closed form solutions

In the design of beam intercepting devices it is very important to know the temperature rise after a single pulse hits a target. Usually the adiabatic temperature rise is computed simply by dividing the obtained energy density deposited at each location in space by the product of the density and specific heat. This overestimates the temperatures but proves to be a good approximation when heat diffusion within the pulselength is negligible which is a valid assumption for a combined case of a short pulselength and small enough temperature gradients. In the case of longer lasting pulses heat diffusion has to be taken into account as the gradients of temperature surrounding the peak of temperature are important. By consequence heat flow towards the coldest regions is no longer negligible. Panels (b), (d) and (f) of Fig. 2 show the sensibility of the peak temperatures in comparison to the adiabatic temperature rise which overestimates the real peak. The presented solutions provide a very good approximation for all dimensional cases and can be applied within MATLAB [20] in just a few seconds using built in functions of the error function and exponential integral. The partial sum solutions need 30 s to a minute depending on the number of terms chosen for the series. One could also use a commercial finite element software like ANSYS [3]. For a usual 3D model composed of 300,000 elements the time necessary to compute the transient temperature field is of the order of 5 min. The above listed times are estimates given for a workstation with two CPU's of frequency 1.2 GHz each composed of two intel i5 cores. Moreover in many applications with beam intercepting devices the size of the beam hence of the energy deposition profile will vary so that an adapted mesh should be used for each separate case. This clearly necessitates more time to prepare the model and the analytic solutions would again prove to be more efficient.

Tables 1 and 2 show the material and beam properties for each case study. These values are used to compute the dimensionless parameters, namely Π_1, Π_2 and Π_3, presented in Section 4. In Table 2 the second column provides the maximum energy deposition, E_{dep} in GeV $\cdot$ cm^{-3} $\cdot$ p^{-1} where p^{-1} denotes per particle, at the end of the pulselength. This energy deposition is provided by FLUKA [7,14]. The fifth column of the same table shows the number of particles that compose the entire beam for the pulselength t_p. These two parameters are necessary for the computation of $A = E_{dep} \cdot n_p \cdot t_p^{-1} \cdot 10^{-4}$. The initial temperature T_i is set to 293.15 K for all three case studies.

6.1. 3D case study: cancer treatment at CNAO

At the National Centre for Oncological Treatment (CNAO) in Pavia, Italy [10] tumors are treated using protons and carbon ion particle beams [2,15]. The beam enters the human body and is set to have a peak energy deposition where the tumor is located.

Table 1
Table describing the material properties for the three case studies presented.

	ρ ($kg \cdot m^{-3}$)	c ($J \cdot kg^{-1} \cdot K^{-1}$)	k ($W \cdot m^{-1} \cdot K^{-1}$)	L (m)
Beryllium window	1860	1776.5	216	0.035
CNAO (Water)	1000	4204	0.6	0.04
SEM grid (Tungsten)	19,250	1300	173	0.04

Since the location of maximum energy deposition will not be at the entrance of the receiving body the energy deposition profile will be different from the beam's profile due to particle scattering. We have conducted FLUKA simulations in order to fit the energy deposition into a Gaussian distribution that is used as a source term in the heat diffusion equation. The human body's composition will be modelled as solely water and the energy deposited will be taken as a three dimensional Gaussian with a standard deviation in all three directions equal to the geometric average of the three standard deviations of the energy profile obtained by FLUKA. We can therefore use the formulations for the three dimensional infinite space solutions developed herein. The parameters needed for the mathematical formulations in Eq. (15) are, $\Pi_1 = 8.9201 \cdot 10^{-5}$, $\Pi_2 = 0.0339$ and $\Pi_3 = 0.026$. Parameters Π_1 and Π_2 in Fig. 2(a) yield a relative energy loss less than 10^{-14} so that the infinite medium solutions for this case study are very accurate in approximating heat diffusion in a confined space. In Fig. 3 are plotted the temperature distributions from the infinite solution as well as from the first 200 terms of the Spherical Bessel series solution, in space for increasing normalized time values. Errors are presented in Table 3 as well as in Fig. 3(b). The non-dimensional peak temperature is of major interest and it can be easily computed using Eq. (18). This value can be compared to the theoretical non-dimensional peak temperature for a zero diffusivity with the ratio $\theta_A(0,1)/\Pi_3 \sim 0.9$. Indeed Π_3 overestimates the real temperature peak by more then eleven percent.

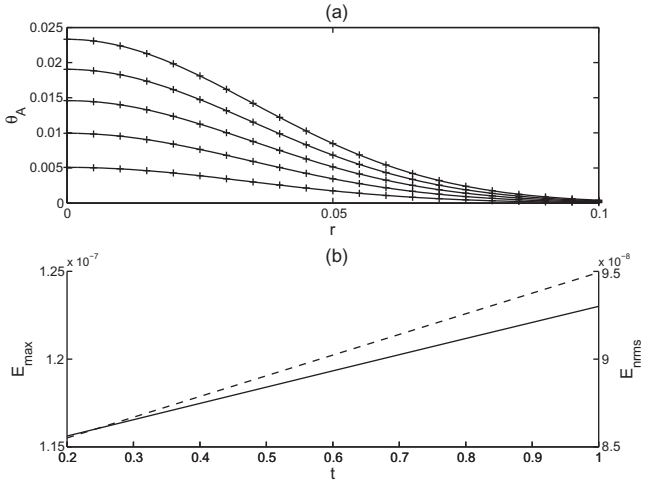

Fig. 3. In panel (a) are shown infinite three-dimensional medium solutions in solid and spherical Bessel series solutions of temperature space distributions in cross marker types, for normalized time $t = 0.2, 0.4, 0.6, 0.8, 1$ such that the lowest curve is for $t = 0.2$ and the highest curve is for $t = 1$. Panel (b) shows E_{nrms} in solid and E_{max} in dashed lines versus normalized time on the abscissa.

Table 3
Table describing the accuracy of the infinite space solutions, the finite space partial sums and the difference between the two.

	$E_L(1)$	N_o terms	$\epsilon_{nrms}(1)$	$E_{nrms}\leqslant$	$E_{max}\leqslant$
Beryllium window	$5.1659 \cdot 10^{-14}$	200	$7.42 \cdot 10^{-4}$	$1.89 \cdot 10^{-6}$	$5.52 \cdot 10^{-6}$
CNAO	$4.45 \cdot 10^{-15}$	200	0.0023	$9.3 \cdot 10^{-8}$	$1.25 \cdot 10^{-7}$
SEM grid	$5.26 \cdot 10^{-13}$	1000	0.0629	$1.09 \cdot 10^{-9}$	$2.03 \cdot 10^{-8}$

6.2. 2D case study: beam window at CERN

The High-Radiation to Materials facility at CERN [5] will allow testing of components of the Large Hadron Collider. These components will be enclosed in a vacuum chamber where the particle beam would enter through specifically designed windows [21]. The beam particles would lose part of their energy through the window's surface with a planar distribution equal to the beam cross-sectional distribution [14]. The thickness of the window is of such measure that one can assume a purely two-dimensional heat diffusion in the radial direction. We can therefore apply the development of two-dimensional solutions to solve for the temperature field on the surface of the window using the following dimensionless parameters, $\Pi_1 = 3.8421 \cdot 10^{-7}$, $\Pi_2 = 0.0143$ and $\Pi_3 = 4.7007$. In Fig. 4 are plotted the temperature distributions from the infinite space solution as well as from the first 200 terms of the Bessel series solution in space for increasing normalized time values. The error parameters defined in Sections 4, 5.4 and 5.5 are presented in Table 3 as well as in Fig. 4(b). The relative energy loss is of the order of 10^{-14} so that the analytic infinite medium solutions are very suitable. This time the ratio $\theta_B(0,1)/\Pi_3 \sim 0.998$ which shows that the adiabatic temperature peak is a good approximation. If one chooses to vary the beam size or the material used for the window this ratio can change drastically as it is shown in panel (d) of Fig. 2.

6.3. 1D case study: SEM Grids

Secondary emission monitors (SEM grids) consist of thin ribbons or wires that individually interact with the beam. Each wire is connected to an acquisition system that permits the reconstruction of the beam profile by taking into account the intensity and temperature through the wires [9]. Temperature calculations are usually made using an adiabatic model where this paragraph suggests that diffusion of heat could be taken into account in order to have a more precise temperature profile through space and time. At high enough energies the beam goes right through the wires and one can assume a one dimensional heat diffusion problem in the direction of the wire. Below is an example of the resultant temperature fields through a wire resulting from a beam impacting the wire. The dimensionless parameters used in the present illustration are computed using [9] and read, $\Pi_1 = 4.3207 \cdot 10^{-7}$,

Table 2
Table describing the beam properties for the three case studies presented.

	E_{dep}	σ (m)	t_p (s)	n_p	A ($W \cdot m^{-3}$)
Beryllium window	0.58	$5 \cdot 10^{-4}$	$7.2 \cdot 10^{-6}$	$4.9 \cdot 10^{13}$	$6.3241 \cdot 10^{14}$
CNAO	100	$1.35656 \cdot 10^{-3}$	1	$2 \cdot 10^{9}$	$3.2044 \cdot 10^{7}$
SEM grid	1.02	10^{-3}	10^{-4}	$4.3691 \cdot 10^{13}$	$7.1401 \cdot 10^{13}$

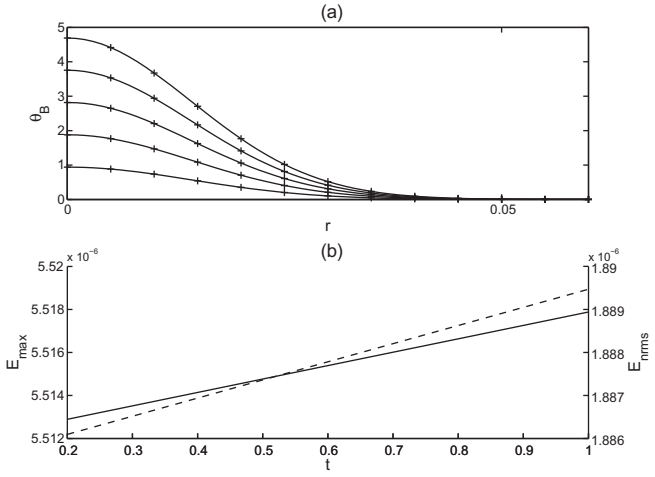

Fig. 4. In panel (a) are shown the infinite two-dimensional medium solutions in solid and Bessel series solutions of temperature space distributions in cross marker types, for normalized time $t = 0.2, 0.4, 0.6, 0.8, 1$ such that the lowest curve is for $t = 0.2$ and the highest curve is for $t = 1$. Panel (b) shows E_{nrms} in solid and E_{max} in dashed lines versus normalized time on the abscissa.

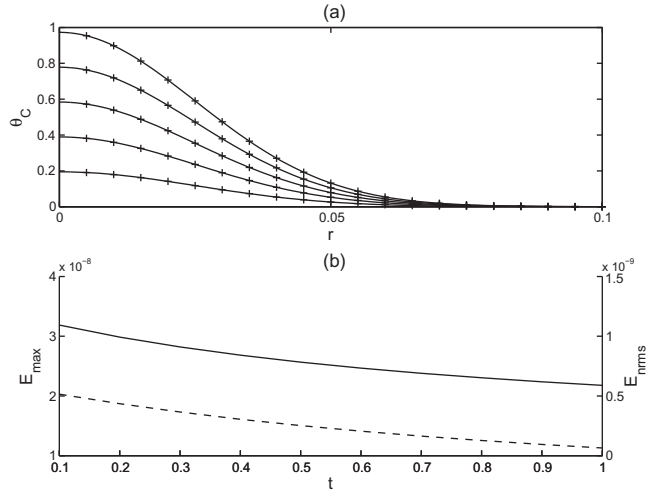

Fig. 5. This figure illustrates the one-dimensional case. In panel (a) are shown infinite medium solutions in solid and Fourier series solutions of temperature space distributions in cross marker types, for normalized time $t = 0.2, 0.4, 0.6, 0.8, 1$ such that the lowest curve is for $t = 0.2$ and the highest curve is for $t = 1$. Panel (b) shows E_{nrms} in solid and E_{max} in dashed lines versus normalized time on the abscissa.

$\Pi_2 = 0.025$ and $\Pi_3 = 0.9733$. Infinite space results are compared to the normalized partial sums in Fig. 5 where Table 3 and Fig. 5(b) confirm the very low relative errors. For the above parameters the ratio $\theta_C(0,1)/\Pi_3 \sim 0.9997$ show that the adiabatic temperature would provide a good approximation.

7. Conclusions

Closed form solutions of the specific non-homogeneous heat diffusion equation are obtained as well as ranges of dimensionless parameters in which the solutions for the infinite medium problem are very good approximations to a bounded medium heat diffusion. The source term is modelled as Gaussian, as can be done for the energy deposition in beam intercepting devices. The above solutions are valid for the time interval of the pulse and therefore yield precise results for maximum temperatures and temperature gradient fields. Provided that the parameters Π_1 and Π_2 are each within a specific range as illustrated in Fig. 2(a), (c) and (e), the infinite domain temperature distributions match very well their finite domain counterparts. The efficiency of this approach versus the infinite series solutions is demonstrated, where the choice of the number of terms in the partial sum for a desired precision is strongly dependant to the values of the three parameters. The use of commercial finite element software would also be more time consuming as one needs to create a geometry and a well adapted mesh before solving the problem.

Moreover the temperature fields at the end of the energy deposition can be used to further analyse the homogeneous diffusion problem with an non-homogeneous initial condition equal to the final distribution of the present one. Furthermore, under some acceptable assumptions the equations of thermoelasticity can be uncoupled such that no displacement terms are present within the final heat equation. One could use the solutions in the present article in order to evaluate the resultant thermoelastic waves [23] where the temperature field acts as a source in the displacement equations.

Finally during the design process of a beam intercepting device where material choices are unclear and beam size might still vary, there is often need of a sensibility and/or optimization analysis. This is much simpler to achieve with analytic solutions then to conduct an iterative process of multiple numerical simulations using a commercial finite element software.

Acknowledgements

The authors thank Richard Craster and Federico Roncarolo for many useful inputs.

Appendix A

The integral in Eq. (3) is separated in two steps. First the space integration is performed where the results can be displayed in a generalized relation for all dimensions then the time integration is performed to obtain the final results shown in Eqs. (4), (6) and (8). Let us start by rewriting the general Green's function for the Heat Diffusion equation as well as the Gaussian source term in a form of a standard normal distribution multiplied by a coefficient,

$$G_n(\mathbf{R},\tau) = H(\tau)\frac{1}{(2\pi 2D\tau)^{n/2}}\exp\left(\frac{-\mathbf{R}^2}{4D\tau}\right), \tag{A.1}$$

$$f(\mathbf{r},t) = \frac{A(2\pi\sigma^2)^{n/2}}{\rho c}\frac{1}{(2\pi\sigma^2)^{n/2}}\exp\left(\frac{-r^2}{2\sigma^2}\right). \tag{A.2}$$

The convolution of two standard normal distributions with zero mean is a standard normal distribution with zero mean and a standard deviation given by $\sigma_{G\circledast f} = \sqrt{(\sigma^2 + 2D\tau)}$ [30]. It follows that,

$$\begin{aligned} I_1 &= \int_V G_n(\mathbf{R},\tau) f(\mathbf{r}',t')dV' \\ &= \frac{A(2\pi\sigma^2)^{n/2}}{\rho c}\frac{1}{(2\pi(\sigma^2+2D\tau))^{n/2}}\exp\left(\frac{-r^2}{2\sigma^2+4D\tau}\right) \qquad (A.3) \\ &= \frac{A\sigma^n}{\rho c(\sigma^2+2D\tau)^{n/2}}\exp\left(\frac{-r^2}{2\sigma^2+4D\tau}\right). \qquad (A.4) \end{aligned}$$

The above equation is true for $n = 1, 2, 3$. For all n we now compute $I_2 = \int_{t_0}^{t} I_1 dt'$ to obtain three relations respectively for the three, two and one dimensional case. Let us use the transformation,

$$\xi = \frac{1}{\sqrt{\sigma^2 + 2D(t-t')}}, \tag{A.5}$$

where $dt' = d\xi/(D\xi^3)$. Without loss of generality we assume $t_0 = 0$ and the limits of integration become $(\sigma^2 + 2Dt)^{-1/2} < \xi < 1/\sigma$. The new relation for I_2 is,

$$I_2 = \frac{A\sigma^n}{k} \int_{(\sigma^2+2Dt)^{-1/2}}^{1/\sigma} \xi^{n-3} \exp\left(\frac{-r^2\xi^2}{2}\right) d\xi \tag{A.6}$$

If $n = 3$ it is trivial to see that Eq. (4) is obtained. For $n = 2$ and the according Eq. (6) one needs to separate the integral into two integrals each with one integration limit at infinity and to apply a different substitution for each new integral namely, $\xi = \sqrt{\zeta}/\sigma$ and $\xi = \sqrt{\zeta}/(\sigma^2 + 2Dt)^{1/2}$. Finally for $n = 1$ integration by parts yields Eq. (8).

The expansion in McLaurin series for the peak temperatures is simple and needs no further explanation.

References

[1] U. Amaldi, History of hadron therapy in the world and italian developments, Riv. Med. 14 (2008) 7–22.
[2] A. Ansarinejad et al., The on-line detectors of the beam delivery system for centro nazionale di adroterapia oncologica (cnao), Nuclear Physics B 197 (2009) 185–189.
[3] ANSYS, 2012. <http://www.ansys.com>.
[4] G. Araya, G. Gutierrez, Analytical solution for a transient, three-dimensional temperature distribution due to a moving laser beam, Int. J. Heat Mass Transfer 49 (2006) 4124–4131.
[5] R. Assmann et al., Specification for a test facility with high power lhc type beam. Tech. rep, 2008.
[6] G. Barton, Elements of Green's Functions and Propagation, Oxford University Press, Oxford, 1989.
[7] G. Battistoni et al., The Fluka Code: Description and Benchmarking, vol. 896, AIP Conference Proceedings, 2007, pp. 31–49.
[8] H. Carslaw, J. Jaeger, Conduction of Heat in Solids, Oxford Science Publications, Oxford, 1959.
[9] B. Cheymol, Development of beam transverse profile and emmittance monitors for the cern linac4, Ph.D. thesis, Université Clermont-Ferrand II – Blaise Pascal.
[10] CNAO, 2001. <http://www.cnao.it>.
[11] D. Couedel et al., 2D-heat transfer modelling within limited regions using moving sources: application to electron beam welding, Int. J. Heat Mass Transfer 46 (2003) 4553–4559.
[12] T. Eagar, N.-S. Tsai, Temperature fields produced by traveling distributed heat sources, Weld. Res. Suppl. 62 (1983) 346–355.
[13] R. Fassani, O. Trevisan, Analytical modeling of multipass welding process with distributed heat source, J. Braz. Soc. Mech. Sci. Eng. 25 (2003) 302–305.
[14] A. Fasso, A. Ferrari, J. Raft, P. Sala, Fluka: status and prospective for hadronic applications, 2001.
[15] S. Giordanengo, Performances of the scanning system for the cnao center of oncological hadron therapy, Nucl. Instrum. Methods Phys. Res. A 613 (2010) 317–322.
[16] R. Haberman, Elementary Applied Partial Differential Equations, Prentice Hall, Englewood Cliffs, New Jersey, 1987. 07632.
[17] J. Kidawa-Kukla, Temperature distribution in a rectangular plate heated by a moving heat source, Int. J. Heat Mass Transfer 51 (2007) 865–872.
[18] M. Lax, Temperature rise induced by a laser beam, J. Appl. Phys. 48 (1977) 3919–3924.
[19] O. Manca, B. Morrone, V. Naso, Quasi-steady-state three-dimensional temperature distribution induced by a moving circular gaussian heat source in a finite depth solid, Int. J. Heat Mass Transfer 38 (1995) 1305–1315.
[20] MATLAB, 2012. <http://www.mathworks.com>.
[21] M. Monteil, J. Blanco, R. Veness, A transparent vacuum window for high-intensity pulsed beams, Vacuum 85 (2011) 1165–1169.
[22] N. Nguyen, A. Ohta, K. Matsuoka, N. Suzuki, Y. Maeda, Analytical solutions for transient temperature of semi-infinite body subjected to 3-d moving heat sources, Weld. Res. Suppl. 78 (1999) 82–92.
[23] W. Nowacki, Dynamic Problems of Thermoelasticity, Noordhoff International Publishing, Leyden, The Netherlands, 1975.
[24] S. Peraire, P. Sala, Beam dumps and beam stoppers for lhc and cngs transfer lines, LHC Project Report 208, 2001.
[25] D. Rosenthal, The Theory of Moving Sources of Heat and Its Applications to Metal Treatments, ASME, 1946.
[26] D. Sanders, Temperature distributions produced by scanning gaussian laser beams, Appl. Opt. 23 (1984) 30–35.
[27] M. Scapin, L. Peroni, A. Dallocchio, in: Damage evaluation in metal structures subjected to high energy deposition due to particle beams, IOP Publishing, 2011.
[28] N. Tahir, R. Schmiddt, M. Brugger, Interaction of super proton synchrotron beam with solid copper target: simulations of future experiments at hiradmat facility at cern, Nucl. Instrum. Methods Phys. Res. Sect. A 606 (2009) 186–192.
[29] G. Tolstov, Fourier Series, Dover Publications, Inc., 180 Varick Street, New York, 1976. 10014.
[30] S. Vinga, J.S. Almeida, Rnyi continuous entropy of dna sequences, J. Theor. Biol. (2004) 377–388.
[31] J. Winczek, Analytical solution to transient temperature field in a half-infinite body caused by moving volumetric heat source, Int. J. Heat Mass Transfer 53 (2010) 5774–5781.